Catalysis Today 161 (2011) 91–96

Contents lists available at ScienceDirect

Catalysis Today

journal homepage: www.elsevier.com/locate/cattod

# Carbon nanotube–$TiO_2$ thin films for photocatalytic applications

Maria J. Sampaio, Cláudia G. Silva, Rita R.N. Marques, Adrián M.T. Silva, Joaquim L. Faria*

*Laboratório de Catálise e Materiais, Laboratório Associado LSRE/LCM, Departamento de Engenharia Química, Faculdade de Engenharia, Universidade do Porto, Rua Dr. Roberto Frias s/n, 4200-465 Porto, Portugal*

ARTICLE INFO

*Article history:*
Received 12 June 2010
Received in revised form
12 November 2010
Accepted 17 November 2010
Available online 15 January 2011

*Keywords:*
Photocatalysis
Carbon nanotubes
Titanium dioxide
Composites
Films
Methylene blue

ABSTRACT

Films made of different types of $TiO_2$ powders and carbon nanotube–$TiO_2$ composites were prepared on a glass substrate by using the doctor blade technique. The electron microscope thin films ranged from 3.75 to 5.00 μm in thickness. Depending on the nature of the $TiO_2$, the composite films containing different amounts of carbon nanotubes evidenced different spectroscopic and morphological properties. The surface roughness was analyzed by atomic force microscopy. The photocatalytic activity of the films was tested in the degradation of methylene blue by near-UV to visible irradiation. The introduction of carbon nanotubes in the $TiO_2$ matrix usually increased the rate of photocatalytic degradation.



## 1. Introduction

Environmental problems associated with effluents (gases or liquids) generated by industries and the development of technologies for treatment of these effluents have provided the driving force for sustained fundamental and applied research in the area of environmental remediation. Heterogeneous photocatalysis by semiconductor materials has been extensively studied and widely applied to environmental purification both in gas and liquid phases [1–4]. This is because the photoactivated semiconductors can completely decompose various kinds of organic pollutants that are refractory, toxic, and nonbiodegradable, to $CO_2$ and $H_2O$ under mild conditions (room temperature and atmospheric pressure) [1,5].

Although titanium dioxide is considered the catalyst of excellence in photocatalysis applications, in particular for the degradation of organic pollutants, it requires excitation in the near UV region (bandgap energy of 3.2 eV), accounting for its low solar efficiency [6–8]. In order to overcome this limitation, the major practices involve catalyst modification by doping metal and nonmetal ions into the $TiO_2$ lattice, dye photosensitization, deposition of noble metals, mixing with other semiconductors, or addition of inert supports [9–14].

It has been reported that carbon materials have some beneficial effects on the photocatalytic activity of $TiO_2$ by inducing synergies or cooperative effects between the metal oxide and carbon phases [11,15–18]. Some recent works have emphasized the preparation of carbon nanotube/titanium dioxide (CNT–$TiO_2$) nanocomposite catalysts aiming at a synergetic combination of their intrinsic properties and thus enhanced performance in the field of heterogeneous photocatalysis [19–21].

The application of photocatalysts as suspensions to treat aqueous effluents can ensure a shorter time for pollutant degradation compared to when they are applied as a film, due to the larger amount of catalyst per unit of volume. However, several practical problems arise from the use of a catalyst in powder form: difficult separation of the catalyst from the suspension, aggregation of its particles at higher catalyst loading on the suspension and the difficulty of applying the method for continuous flow systems. One way of circumventing these drawbacks is by using coatings or films on support surfaces where the catalyst particles are immobilized [22–25].

In this work, CNT–$TiO_2$ materials were immobilized as thin films on glass slides by using the so-called doctor blade method which can be easily employed as a fast and nonenergy consuming technique for mass production of thin films with good uniformity and reproducible properties. Our goals are to produce CNT–$TiO_2$ films with different morphologies at the micro/nano scale and to study their performance in photocatalytic oxidation reactions in aqueous media. Films produced using different $TiO_2$ sources and differ-

* Corresponding author.
*E-mail address:* jlfaria@fe.up.pt (J.L. Faria).

0920-5861/$ – see front matter © 2011 Elsevier B.V. All rights reserved.
doi:10.1016/j.cattod.2010.11.081

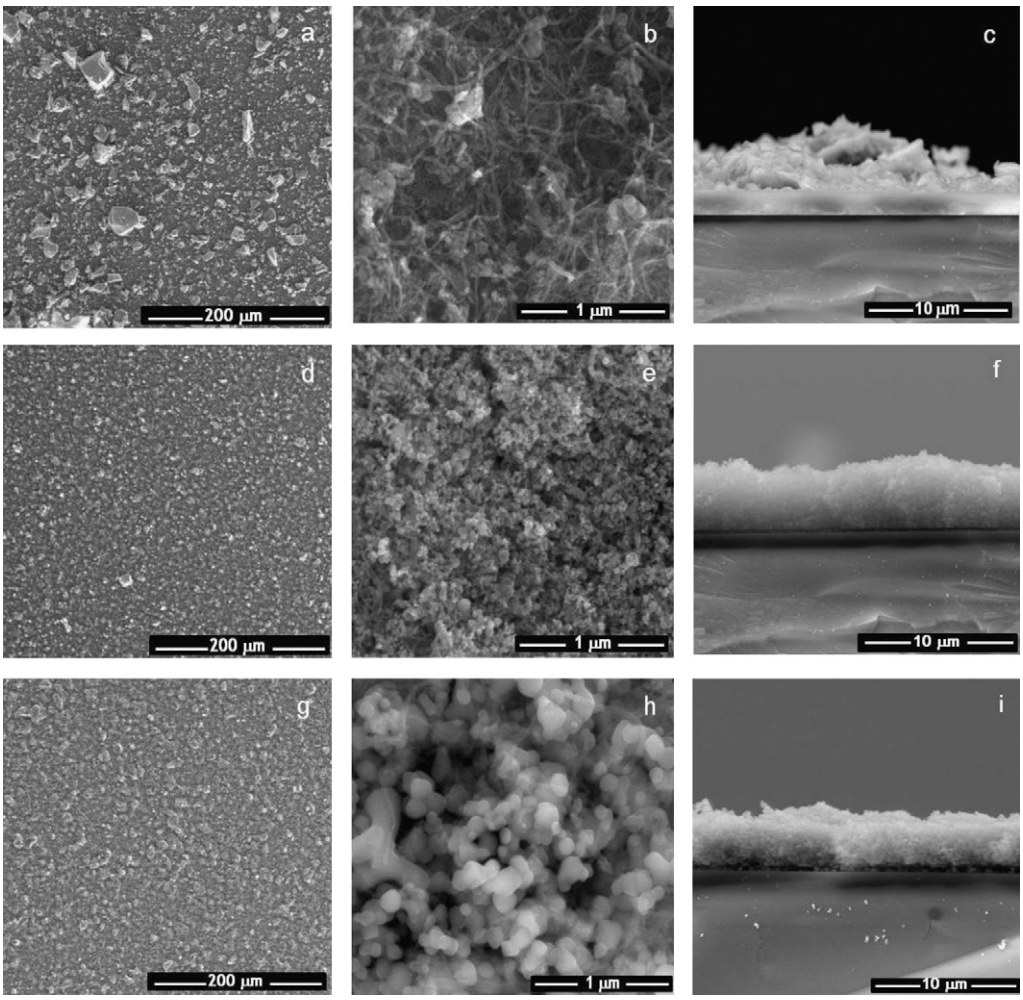


**Fig. 1.** SEM images of SG/CNT-20 (a), (b) and (c), EP/CNT-20 (d), (e) and (f), and SA/CNT-20 (g), (h) and (i). Figures (c), (f) and (i) are sectional cuts of the films.

ent CNT contents were used in the photocatalytic degradation of methylene blue (MB) in aqueous solutions, which is a commonly used model compound for photocatalyst screening reactions using $TiO_2$-based films [26,27].

## 2. Experimental

### 2.1. Reagents and materials

Titanium (IV) isopropoxide ($Ti[OCH(CH_3)_2]_4$, 97%), titanium (IV) oxide powder anatase ($TiO_2$, 99.8% metal basis), nitric acid ($HNO_3$, ≥65%), methylene blue hydrate ($C_{16}H_{18}ClN_3S{\cdot}xH_2O \geq 95\%$), α-terpineol ($C_{10}H_{18}O$, 90%), acetone ($CH_3COCH_3 \geq 99.5\%$) and ethylcellulose were purchased from Sigma–Aldrich. Ethanol ($C_2H_5OH$, 99.5%) was obtained from Panreac. Ultrapure water was produced in a Direct-Q millipore system. $TiO_2$ Aeroxide P-25 was supplied by Degussa AG (now Evonik). Multi-walled carbon nanotubes were purchased from Shenzhen Nanotech Port Co. Ltd. (manufacturer data: purity > 95%, diameter < 10 nm, length = 5–15 μm; ash content ≤ 0.2 wt.%, surface area = 40–300 $m^2\,g^{-1}$, amorphous carbon < 3%). The measured BET surface area (see below for measurement details) of the original carbon nanotubes was 100 $m^2/g$.

### 2.2. Catalyst preparation

Before being used, carbon nanotubes were functionalized in a 10 M $HNO_3$ solution at boiling temperature for 3 h. After cooling, the CNT were recovered by filtration, rinsed with distilled water up to neutral pH and dried overnight at 110 °C. The BET surface area of the functionalized CNT (see below for measurement details) was 160 $m^2/g$.

CNT–$TiO_2$ composite catalysts were prepared by mixing $TiO_2$ (commercial or previously synthesized by a sol–gel method as described elsewhere [28]) with the CNT phase by using a hydration–dehydration technique [21]. Firstly, the functionalized CNT were dispersed in water under ultrasonication. The $TiO_2$ powder was added 30 min later to the suspension and the mixture was heated up to 80 °C and magnetically stirred until the water was completely evaporated. The obtained composite was dried overnight at 110 °C to eliminate the remaining humidity before being stored.

The composite materials were obtained by using different types of $TiO_2$ and different CNT loadings. Catalysts were labeled as XX/CNT-Y, where "XX" corresponds to the type of $TiO_2$ ("EP" for Evonik P25, "SA" for $TiO_2$ obtained from Sigma–Aldrich and "SG" for $TiO_2$ produced by the sol–gel procedure) and "Y" corresponds to the weight ratio of CNT in a 100 weight basis of neat $TiO_2$. For instance, SG/CNT-20 means (100)SG:(20)CNT w/w, where the amount of $TiO_2$ is 5 times higher than the one of CNT.

EP has been widely used in numerous photocatalytic studies being generally accepted as the benchmark catalyst for photooxidation reactions. It is constituted by 80% of anatase phase and 20% of rutile (manufacturer data). Both SA and SG are constituted by pure anatase $TiO_2$ nanoparticles.

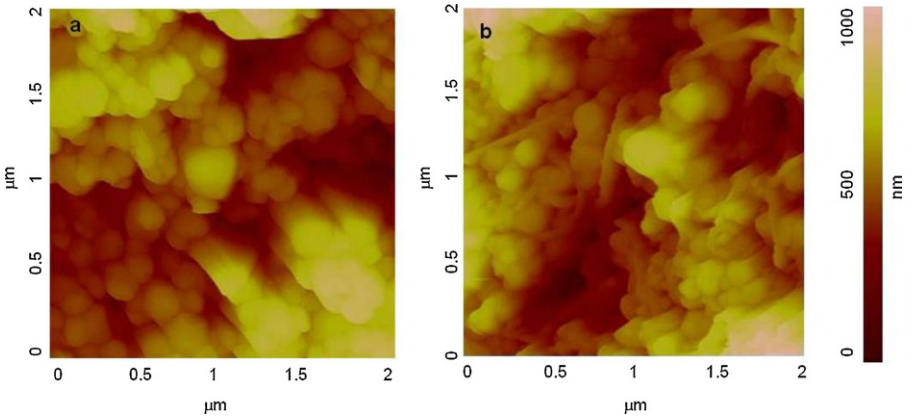


**Fig. 2.** AFM images of SA (a) and SA/CNT-20 (b) films.

### 2.3. Film preparation

Glass slides of 1.5 cm diameter coated on one side with different pastes of each material were used to prepare thin films. To remove contaminants, glass slides were cleaned with distilled water containing an anionic detergent and subsequently washed exhaustively with milli-Q water and sonicated for 15 min. Then the slides were immersed in acetone and sonicated for 15 min. The same procedure was repeated using isopropanol.

A paste of each powder material was prepared by mixing 50 mg of the respective solid with 1.5 mL of a solution constituted by acetone (10.0 mL), α-terpineol (5.0 mL) and ethylcellulose (0.3 g). The mixture was left under stirring during 24 h in a closed vial. After that period, the vial was opened for solvent evaporation under stirring for another 24 h. Each paste was spread on a freshly cleaned transparent glass slide using the doctor blade technique.

The surface to be covered by the semiconductor was defined by two parallel stripes of one layer Scotch® adhesive tape as a spacer to obtain approximately the same film thickness. The area obtained was of 1.0 $cm^2$. After the tape was removed, the glass plates were calcined at 450 °C for 1 h. The original CNT are stable at this temperature, as confirmed by thermogravimetric analysis.

### 2.4. Characterization techniques

The UV–Vis spectra of the powder solids and films were measured on a Jasco V-560 UV–Vis spectrophotometer, equipped with an integrating sphere attachment (JASCO ISV-469). The spectra were recorded in diffuse reflectance mode and transformed by the instrument software (JASCO) to equivalent absorption Kubelka–Munk units. Observations of the surface morphology and roughness of the films were performed using scanning electron microscopy (SEM) FEI Quanta 400FEG ESEM/EDAX Genesis X4M instrument. The SEM apparatus was equipped with a special multiple sample holder, in which the broken glass slides were vertically positioned to observe and measure the cross-section of the catalyst films by using SEM instrument software. Atomic force microscopy (AFM) was performed on a Veeco Metrology Nanoscope IVA atomic force microscope, operating in tapping mode. The specific surface area ($S_{BET}$) of the powder materials was determined by multipoint analysis of $N_2$ adsorption isotherms at 77 K using BET method, with a Quantachrome NOVA 4200e multi-station apparatus.

### 2.5. Photodegradation experiments

The films were used in the photocatalytic degradation of methylene blue (MB) in aqueous solution. The photocatalytic experiments were performed in a glass cylindrical reactor filled with 6.5 mL of a 10 ppm MB aqueous solution. The solution was magnetically stirred and continuously purged with an oxygen flow. The irradiation source consisted in a Heraeus TQ 150 medium-pressure mercury vapor lamp ($\lambda_{exc}$ = 254, 313, 366, 436 and 546 nm). A DURAN® glass cooling jacket was used for irradiation in the near-UV to visible light range ($\lambda_{exc}$ = 366, 436 and 546 nm). The lamp was located 6 cm from the films. Light intensity at this position was approximately 50 mW $cm^{-2}$. The maximum temperature reached during the pho-

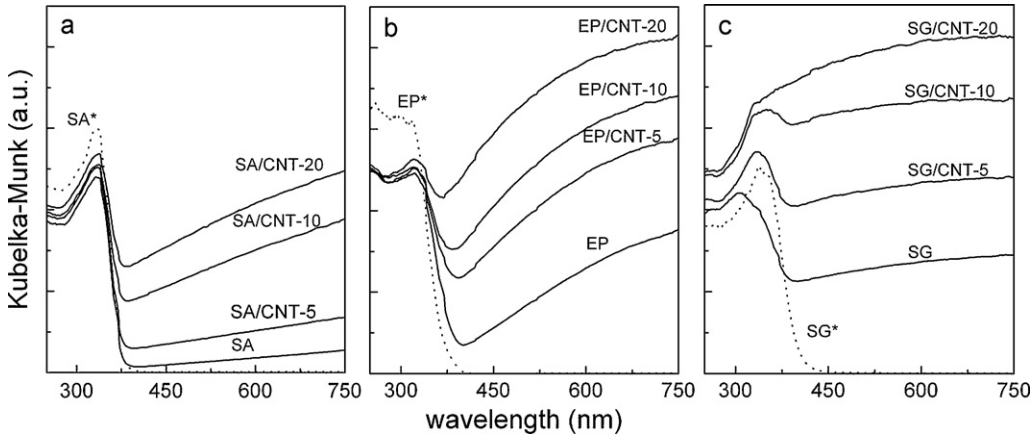


**Fig. 3.** Diffuse reflectance UV–Vis spectra of SA (a), EP (b) and SG (c) films. SA*, EP* and SG* are the spectra of the corresponding powder substrates.

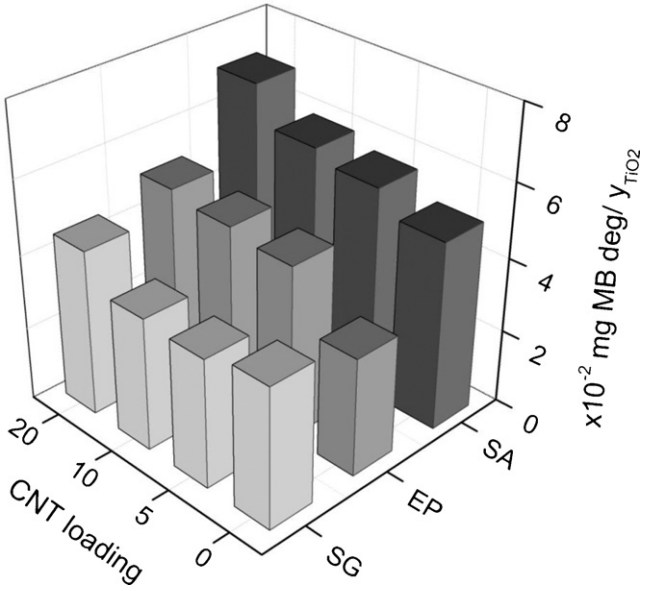


**Fig. 4.** MB conversion after 60 min of irradiation using SG, EP and SA based materials.

tocatalytic experiments was of 35 °C. The illuminated area on the films was kept at 0.79 $cm^2$ and was delimited by using a Viton® o-ring.

Before turning illumination on, the solution was magnetically stirred in the dark for 15 min, to establish an adsorption–desorption equilibrium. The adsorption capacity of $TiO_2$ films was around 4% of the initial amount of MB and less than 10% for all the composites. Then, the solution was irradiated with near-UV to visible light at constant stirring speed. The first sample was taken out at the end of the dark adsorption period, just before the light was turned on, in order to determine the MB concentration in solution, which was hereafter considered as the initial concentration ($C_0$) after dark adsorption. Samples were then withdrawn regularly from the reactor and analyzed by UV–Vis spectrophotometry in a Jasco V-560 spectrophotometer. Selected experiments were repeated in order to check the reproducibility of the obtained results.

For comparison purposes, reactions using catalyst suspensions were also performed. In that case, the amount of catalyst was kept at 1 mg in 6.5 mL of MB solution. Reaction in the absence of catalyst was performed as a blank experiment in order to characterize the pure photochemical regime.

## 3. Results and discussion

### 3.1. Film characterization

Scanning electron microscopy allows the visualization of the morphology of the catalyst films deposited on the glass slides. Fig. 1 shows representative SEM micrographs of the films obtained using the CNT–$TiO_2$ composites with higher percentages of CNT. These images clearly reveal the differences in the particle size, uniformity and shape of the particles of the composite materials. SEM images show that relatively homogeneous films at the microscale were obtained when EP (Fig. 1d and e) and SA (Fig. 1 g and h) were used as titanium dioxide phase. However, for SG composites it was observed the presence of particles of relatively large dimensions settled at the surface of the substrate (Fig. 1a and b). Higher magnification micrographs show the typical morphology of CNT–$TiO_2$ composite materials with $TiO_2$ particles surrounding carbon nanotubes. From the SEM images it could also be observed the presence of $TiO_2$ phases with different particle sizes and morphologies.

Typically, SG is constituted by very small anatase crystals of around 10 nm aggregated as larger particles [18]. SEM images of the composites prepared with SG reveal that carbon nanotubes are located mainly at the surface of these large $TiO_2$ particles, as can be observed in Fig. 1b. Using HR-TEM analysis (not shown), it was possible to verify that in the SG/CNT composites a few particles are distributed on the CNT surface and most of them form big aggregates. In the case of EP/CNT composite films, the $TiO_2$ phase reveals a more uniform nanoparticle size distribution centered at 30 nm, with the carbon phase (CNT) homogeneously distributed into the metal oxide matrix (Fig. 1e). This uniform morphology was also observed in the case of SA/CNT films. In Fig. 1h a high magnification image of a region on the SA/CNT-20 film shows the presence of $TiO_2$ particles with sizes in the order of hundreds of nanometers, homogeneously embedding carbon nanotubes. This film is in fact the more homogeneous, well structured and thinner (Fig. 1g–i).

The thickness of the films was determined from SEM micrographs by measuring the cross section of sliced films over many samples. As discussed previously, since the films prepared with SG are very heterogeneous and mechanically unstable it is only possible to refer an estimated thickness, which in the case of SG/CNT-20 (Fig. 1c) was about 5.0 μm (with 8.00 μm at the maximum thickness and 3.00 μm at the minimum). For EP/CNT-20 and SA/CNT-20 the thickness of the films measured from the cross sectional cuts was of 4.50 and 3.75 μm, respectively (Fig. 1f and i).

Surface roughness of selected films was evaluated by atomic force microscopy. Fig. 2 shows the images obtained for SA and SA/CNT-20 films. For these films, the measured surface roughness was of 151 and 156 nm, respectively. These results indicate that the presence of carbon nanotubes do not affect significantly the film surface which means that carbon nanotubes are well dispersed in the $TiO_2$ media. In particular for these films, the roughness values are of the same order of the SA particle dimension, confirming the uniformity of the film surface.

One of the most important characterization procedures for materials used in photocatalytic applications consists in the determination of the optical absorption spectrum. Fig. 3 shows the diffuse reflectance UV–Vis spectra of the films prepared on glass substrates. For comparison purposes, the spectra of the three $TiO_2$ powders (dashed lines) are also shown. As expected, $TiO_2$ powders show the characteristic absorption sharp edge rising at around 400 nm. However, we could observe that $TiO_2$ films show optical absorption for wavelengths higher than the typical absorption

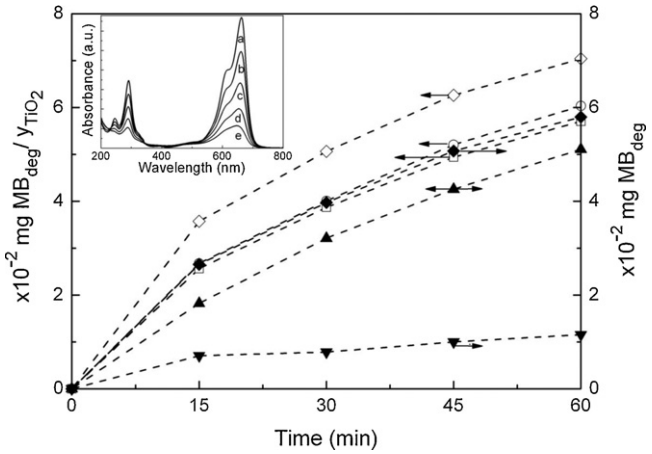


**Fig. 5.** MB degraded during photolytic (–▼–) and photocatalytic reactions using SA (–▲–), SA/CNT-5 (–□–), SA/CNT-10 (–○–), SA/CNT-20 (–◇– and –◆–). Open and filled symbols correspond to normalized (per $y_{TiO2}$) and non-normalized results, respectively. Inset: UV–Vis spectra of MB at 0 min (a), 15 min (b), 30 min (c), 45 min (d) and 60 min (e) of irradiation using SA/CNT-20 as photocatalyst.

edge, this absorption increasing following the order SG > EP > SA. Nevertheless, this behavior was already expected since the films show some light transparency, which can be related both to their thickness and homogeneity.

It is noticeable for all cases that the introduction of CNT into the $TiO_2$ matrix leads to an increase in the optical absorption mainly in the visible spectral range.

The increase in light absorption appears to be proportional to the CNT loading. Additionally, as can be observed in Fig. 3, the introduction of CNT leads to an increase in the absorption edge, which indicates a decrease in the bandgap energy for the composite materials. These observations are in agreement with results reported for CNT–$TiO_2$ composite powders [13,17,19], the increase in the absorption being attributed to the creation of an electronic interphase interaction between CNT and $TiO_2$.

### 3.2. Photocatalytic degradation reactions

The efficiency of the prepared films was evaluated for the photocatalytic degradation of MB under near-UV to visible light irradiation. Since we are irradiating at $\lambda \geq 366$ nm and MB shows absorption in this wavelength range, a photodegradation reaction, in the absence of catalyst, was performed in order to quantify the amount of dye degraded by the photochemical route. At these conditions, it was observed a decrease in MB concentration of less than 20% at the end of 60 min of irradiation.

Photocatalytic degradation of MB was performed by using films of both pure $TiO_2$ and CNT–$TiO_2$ composites, obtained with different types of titanium dioxide and different CNT loadings. Since the amount of $TiO_2$ in each material is different, the MB removal at different reaction times was divided by the mass fraction of the $TiO_2$ phase ($y_{TiO_2}$) in the composite, as follows:

$$\frac{MB_{deg}}{y_{TiO_2}} = \frac{(C_0 - C_t) \times V}{(100)/(100 + Y)} \quad (1)$$

where $C_0$ is the initial concentration of MB, $C_t$ is the concentration at time $t$, $V$ is the volume of the solution used for the photocatalytic reaction and $Y$ is the CNT mass fraction in the composite. The results were therefore quantified in terms of the amount of MB degraded per mass fraction of $TiO_2$ ($y_{TiO_2}$) in each catalyst. Fig. 4 summarizes the results obtained using SG, EP and SA-containing films.

Results show that in most cases there is an increase in the photoefficiency when CNT are present in the films. For EP and SA containing films, this increase in the activity for MB removal was proportional to the CNT loading. In the case of SG-films, no effect was observed when low amounts of CNT were used. Nevertheless, for SG/CNT-20, an increase in the efficiency of about 20% was obtained when comparing with the analogous $TiO_2$ film. However, among the tested films, those containing SG presented the lowest efficiencies than the ones produced using SA and EP, which can be attributed to the lower homogeneity of the resulting films.

SA films have shown the highest efficiencies, with the SA/CNT-20 being the most efficient material. These good results obtained for SA-containing materials can be attributed to both the homogeneity of the obtained films and to the photocatalytic properties of the composite materials. The interaction between CNT and $TiO_2$ phases in the composite materials also depends on key aspects such as $TiO_2$ particle size, $TiO_2$ crystalline phase composition and surface chemistry of both CNT and $TiO_2$. In EP anatase and rutile crystalline phases are both present, and they can interact in a synergic way, accounting for the observed photocatalytic activity of EP–$TiO_2$ composites. Since SA and SG consist only of anatase crystalline phase, the lower activity found for SG-$TiO_2$ composites may result from aggregation of the SG very small particles, leading to a weak interaction with the CNT phase. Fig. 5 shows the time conversion plots of MB degradation in the presence of SA, SA/CNT-5, SA/CNT-10 and SA/CNT-20 catalyst films. For comparison purposes the data obtained for the photolytic reaction are also presented. From Fig. 5 it can be seen that the kinetics of MB removal increase when the composite catalyst films are used.

In Fig. 5 inset is shown the evolution of the spectra of the aqueous solution during the photocatalytic reaction using SA/CNT-20 film. After 60 min of irradiation, a decrease in MB concentration of 89% was observed using this catalyst, which is considerably higher than the 79% of MB removal, obtained with the film prepared with pure SA. It can also be observed in Fig. 5 that even without normalizing the data for MB removal using SA/CNT-20 per mass fraction of $TiO_2$, the observed MB removal was higher than the obtained with SA.

Globally, the results obtained indicate that a synergy effect exists between CNT and $TiO_2$ phases, leading to an increase in the efficiency for MB removal. Results obtained using suspensions of the same catalysts (not shown) revealed a similar tendency as when films were used, *i.e.*, the highest efficiencies were obtained for SA-containing catalysts. However, the optimal CNT loading when using CNT–$TiO_2$ composites in suspension were in some cases different that those obtained for films. In the case of EP materials, the maximum efficiency was obtained for EP/CNT-10. At the end of 60 min of irradiation the conversion of MB using EP and EP/CNT-10 were of $6.4 \times 10^{-2}$ and $7.5 \times 10^{-2}$ mg MB/$y_{TiO_2}$, respectively. For SA and SG materials, the composite catalysts with the highest CNT loading were the most efficient, with MB removals of $6.5 \times 10^{-2}$ and $7.8 \times 10^{-2}$ mg MB/$y_{TiO_2}$ obtained for SA and SA/CNT-20 and of $4.9 \times 10^{-2}$ and $5.3 \times 10^{-2}$ mg MB/$y_{TiO_2}$ for SG and SG/CNT-20, respectively. These results may indicate that the photoefficiency of the composite catalysts cannot only be attributed to the intrinsic properties of the materials but also to the characteristics of the films.

When using photocatalyst suspensions the optimal CNT loading corresponds to the amount of CNT in the composite that leads to the higher catalyst activity, *i.e.*, to the maximum of synergy effect between CNT and $TiO_2$ phases. For higher CNT loadings, the increasing amount of carbon nanotubes may cause light scattering, leading to a decrease of the photoefficiency of the process. In the case of CNT–$TiO_2$ films, this occurrence is avoided by the immobilization of the catalysts on the glass slides.

Studies using CNT–$TiO_2$ slurries have suggested that the role of the CNT phase in the composite catalyst can be ascribed to three distinct mechanisms: (i) CNT may act as a dispersing media for $TiO_2$ nanoparticles; (ii) CNT can act as a co-adsorbent; or (iii) CNT can act as a photosensitizer [13,19,20]. The first mechanism is more significant when $TiO_2$ particles are generated simultaneously during the synthesis of the composite catalyst. In this case, chemical groups at the surface of the CNT may act as anchoring points to $TiO_2$ nanoparticles.

The introduction of high amounts of CNT in the composite catalysts leads to an increase of the $S_{BET}$ of the materials, which can be attributed to a better dispersion of $TiO_2$ particles avoiding the formation of aggregates. The specific surface areas of EP, SA and SG were of 56, 13 and 99 $m^2 g^{-1}$, while for the corresponding composite materials with the highest CNT loading ($TiO_2$/CNT-20) these values increased to 73, 25 and 108 $m^2 g^{-1}$, respectively. In the photocatalytic reactions using CNT–$TiO_2$ films, it was observed for all cases a maximum decrease of 10% in the concentration of MB after the dark adsorption period. Being so, it is not reasonable to ascribe the beneficial effect promoted by CNT to its action as a co-adsorbent. Therefore, it is more reasonable to attribute the positive effect resulting from the presence of CNT in the composite material to its action as a photosensitizer, promoting electric charge transfer between the two phases, reducing the bandgap of the resulting composite catalyst and thus

increasing the efficiency of the photocatalytic process. For the composite films the synergy effect was in general proportional to the increase in the absorbance observed for these materials mainly in the visible spectral range, which supports the creation of an electronic interphase interaction between CNT and the semiconductor.

## 4. Conclusions

$TiO_2$ and CNT–$TiO_2$ composites immobilized in glass slides by the doctor blade technique show photocatalytic activity for the degradation of MB in aqueous media under irradiation in the near-UV to visible spectral range. The photoefficiency of the immobilized catalysts appear to be related to the inherent properties of the materials and to the characteristics of the resulting films. SA-containing films show higher efficiency for the photocatalytic degradation of MB than SG and EP-based ones, which is attributed to the physical–chemical and optical properties of these materials as well as to the higher homogeneity of these films. Kinetics of MB photodegradation is improved by the use of CNT–$TiO_2$ composites. This increase in the photoefficiency is attributed to the creation of an electronic interphase interaction between CNT and $TiO_2$ phases, which leads to a decrease in the bandgap energy of the composite material.

## Acknowledgements

Financial support for this work was provided by national research grants FCOMP-01-0124-FEDER-008442 and REEQ/1106/EQU/2005, by LSRE/LCM LA financing from "Programa de Financiamento Plurianual de Unidades de I&D/Laboratórios Associados" by Fundação para a Ciência e a Tecnologia (FCT), and from the European Commission (Clean Water – Grant Agreement Number 227017), for which the authors are thankful. Clean Water is a Collaborative Project co-funded by the Research DG of the European Commission within the joint RTD activities of the Environment and NMP Thematic Priorities. CGS acknowledges her Post-Doc scholarship by FCT (SFRH/BPD/48777/2008). RRNM thanks FCT for her Doctoral scholarship (SFRH/BD/65425/2009). AMTS acknowledges financial support from POCI/N010/2006.

## References

[1] U.I. Gaya, A.H. Abdullah, J. Photochem. Photobiol. C 9 (2008) 1–12.
[2] J.M. Herrmann, Catal. Today 53 (1999) 115–129.
[3] J. Peral, X. Domenech, D.F. Ollis, J. Chem. Technol. Biotechnol. 70 (1997) 117–140.
[4] J. Zhao, X.D. Yang, Build. Environ. 38 (2003) 645–654.
[5] P.R. Gogate, A.B. Pandit, Adv. Environ. Res. 8 (2004) 501–551.
[6] O. Carp, C.L. Huisman, A. Reller, Prog. Solid State Chem. 32 (2004) 33–177.
[7] A. Fujishima, T.N. Rao, D.A. Tryk, J. Photochem. Photobiol. C 1 (2000) 1–21.
[8] D. Robert, S. Malato, Sci. Total Environ. 291 (2002) 85–97.
[9] F. Kiriakidou, D.I. Kondarides, X.E. Verykios, Catal. Today 54 (1999) 119–130.
[10] M.J. Lopez-Munoz, R. van Grieken, J. Aguado, J. Marugan, Catal. Today 101 (2005) 307–314.
[11] C.G. Silva, J.L. Faria, J. Photochem. Photobiol. A 155 (2003) 133–143.
[12] J.C. Tristao, F. Magalhaes, P. Corio, M.T.C. Sansiviero, J. Photochem. Photobiol. A 181 (2006) 152–157.
[13] W.D. Wang, P. Serp, P. Kalck, J.L. Faria, Appl. Catal. B 56 (2005) 305–312.
[14] X.W. Zhang, M.H. Zhou, L.C. Lei, Appl. Catal. A 282 (2005) 285–293.
[15] J. Matos, J. Laine, J.M. Herrmann, Appl. Catal. B 18 (1998) 281–291.
[16] J. Matos, J. Laine, J.M. Herrmann, J. Catal. 200 (2001) 10–20.
[17] W.D. Wang, P. Serp, P. Kalck, J.L. Faria, J. Mol. Catal. A: Chem. 235 (2005) 194–199.
[18] W.D. Wang, C.G. Silva, J.L. Faria, Appl. Catal. B 70 (2007) 470–478.
[19] B. Gao, G.Z. Chen, G.L. Puma, Appl. Catal. B 89 (2009) 503–509.
[20] C.G. Silva, J.L. Faria, ChemSusChem 3 (2010) 609–618.
[21] Y. Yao, G. Li, S. Ciston, R.M. Lueptow, K.A. Gray, Environ. Sci. Technol. 42 (2008) 4952–4957.
[22] F. Bosc, A. Ayral, P.A. Albouy, C. Guizard, Chem. Mater. 15 (2003) 2463–2468.
[23] D.D. Dionysiou, A.A. Burbano, M.T. Suidan, I. Baudin, J.M. Laine, Environ. Sci. Technol. 36 (2002) 3834–3843.
[24] M. Koelsch, S. Cassaignon, C.T.T. Minh, J.F. Guillemoles, J.P. Jolivet, Thin Solid Films 451 (2004) 86–92.
[25] M. Langlet, A. Kim, M. Audier, C. Guillard, J.M. Herrmann, Thin Solid Films 429 (2003) 13–21.
[26] T.-D. Nguyen-Phan, V.H. Pham, T.V. Cuong, S.H. Hahn, E.J. Kim, J.S. Chung, S.H. Hur, E.W. Shin, Mater. Lett. 64 (2010) 1387–1390.
[27] J. Zita, J. Krysa, A. Mills, J. Photochem. Photobiol. A 203 (2009) 119–124.
[28] C.G. Silva, J.L. Faria, Photochem. Photobiol. Sci. 8 (2009) 705–711.